LAWRENCE
LIVERMORE
NATIONAL
LABORATORY

LLNL-PROC-648150

Effects of Powder Morphology and Particle Size on CT Number Estimates

J. S. Kallman, S. DePiero, S. Azevedo, H. E. Martz

January 6, 2014

Electronic Imaging 2014
San Francisco, CA, United States
February 2, 2014 through February 6, 2014

Disclaimer

Effects of Powder Morphology and Particle Size on CT Number Estimates

Jeffrey S. Kallman*, Sabrina DePiero, Stephen Azevedo, Harry E. Martz, Jr.
Lawrence Livermore National Laboratory, P.O. Box 808, Livermore, CA, USA 94551

IM # 768411

ABSTRACT

We performed experiments and data analysis to determine how powder morphology and particle size affect X-ray attenuation (CT number or CTN). These experiments were performed on a CT system with an isotropic resolution of $(0.15\ mm)^3$, and an endpoint energy of 160kV. Powders with effective atomic number (Z_e) within ±0.2 of water were found to have CTN more directly related to electron density than to bulk physical density. Variations in mean particle size ranging between 2 μm and 44 μm were found to have no effect on specimen mean CTN.

Keywords: X-ray attenuation, particle size, powder packing, electron density

1. INTRODUCTION

Recent measurements of X-ray features of powdered materials raised questions about the effects of powder microstructure on computed tomography (CT) results. The CT number (CTN), which was thought to be directly proportional to physical density, did not produce the values expected relative to a water baseline.

Given these results, we were asked to explore this anomaly in the X-ray signatures for non-liquid materials, particularly powders. This report presents the results and conclusions of this powder study. The key questions to be answered in the study were:

- Why do powders whose physical properties (effective atomic number and density) are near water produce CTN values that do not match those of water?
- How do morphology and particle size of powders affect CTN values?

We proposed a research plan to answer these questions through a set of experiments with two benign powders. We hypothesized that

1. X-ray attenuation would track more accurately with electron density than bulk physical density at the energies and path-lengths being studied;
2. Neither morphology or particle size would cause mean CTN differences if the powders were packed to the same density;

Throughout this report, it is important to note the distinction between two quantities:

- *physical density* or ρ, in units of grams per cubic centimeter (g/cc), is measured by dividing mass by volume; it is also sometimes called bulk or volume density;
- *electron density* or ρ_e, in units of moles of electrons per cubic centimeter (mole-e^-/cc), is measured by X-ray attenuation in the energy range of interest; electron density is a function of the elemental makeup and physical density of the material.

While physical density can be easily measured, it is the effective atomic number and electron density that governs the physics of X-ray interaction with materials. A way to calculate electron density for a material of known composition and physical density is by using a software application called ZeCalc that is available from LLNL[1]. ZeCalc uses X-ray attenuation cross-sections to calculate the material's effective atomic number $(Z_e)^2$ and ρ_e.

* kallman1@llnl.gov; phone 1 925 423-2447

For these powder studies, the effective atomic number of each specimen is within 0.2 of that of water. These small differences in Z_e are not expected to significantly influence the measured CTN values, even when using low-energy CT that is dominated by atomic composition. For this reason, we only studied the high-energy (160kV endpoint energy) CT results, which are primarily electron-density dependent.

2. BACKGROUND

As a way of comparing CT systems in a standard feature space, the X-ray attenuation measurements are often reported in Livermore Modified Hounsfield Units (LMHU), which scale the high-energy CTNs to known values for air (0 LMHU) and water (1000 LMHU). Because the bulk physical density of water is 1 g/cc, and the CTN is related to physical density, it is usually assumed that

$$\mathrm{CTN} = 1000\,\rho. \tag{1}$$

Equation 1 says that for any material effective atomic number near that of water and with $\rho = 1$ g/cc (the same as water), we would expect its CTN to equal 1000 LMHU. For non-liquid materials such as powders or foams that have a particle microstructure and that can be packed to the same physical density as water, the CTN is expected to equal 1000 LMHU.

However, Equation 1 is an approximation that is not always true for every material—liquid or non-liquid. The questions posed were, "Are deviations from Equation 1 caused by some characteristic of powders?" Possible powder characteristics of interest are

- Morphology or particle shape;
- Particle size distribution; and/or
- State of agglomeration of the particles.

These characteristics can affect both the packing density (how tightly compressed the powder is) and the physical density, ρ. Perhaps there should be another term included in Equation 1—*e.g.*, a factor M—that represents these powder characteristics such as:

$$\mathrm{CTN} = 1000\,\mathrm{M}\,\rho. \tag{2}$$

Equation 2 shows a linear relationship between powder characteristics and CTN, but there could be a more complex functional relationship based on morphology, particle size, and/or agglomeration.

An alternative hypothesis for powders that have an effective atomic number close to that of water, is that CTN has a linear relationship with electron density, ρ_e, as follows:

$$\mathrm{CTN} \approx 1000 \left(\frac{\rho_\mathrm{e} \text{ of specimen packed to 1 g/cc}}{\rho_\mathrm{e} \text{ of water}} \right) \rho\ . \tag{3}$$

In words, when a specimen is packed to a physical density of 1 g/cc, its CTN will only equal 1000 if its electron density is equal to the electron density of water. Water has a physical density of 1 g/cc and an electron density of 0.555 mole-e^-/cc. If a powder such as tartaric acid is packed to a bulk physical density of 1 g/cc, ZeCalc estimates its electron density to be 0.52 mole-e^-/cc. In this case, Equation 3 would predict that the CTN of tartaric acid will be less than 1000 when packed to 1 g/cc.

3. RESEARCH PLAN

The research reported here was undertaken to experimentally examine the deviation of CTN values of powders measured on a CT scanner at LLNL. Our goal was to investigate the relationship between powder characteristics and CT attenuation by examining specimens composed of two different powders. The scans were designed to determine if the CTN deviation effect is caused by powder characteristics as given in Equation 2 or by the electron density ratio as indicated by Equation 3.

4. POWDER MATERIALS

For this study, we chose to scan two powders whose effective atomic numbers are similar to water. The powders were *tartaric acid* ($C_4H_6O_6$) and *lithium carbonate* (Li_2CO_3), which are both readily-available white powders. Tartaric acid is a powder (Z_e = 7.24 and = 0.52 mole-e^-/cc when packed to a physical density of 1 g/cc) with a wide particle-size variation. Tartaric acid particles can be milled into smaller sizes so that we can evaluate the same powder with the same physical density but with different particle sizes. Lithium carbonate is another white powder (Z_e = 7.27 and = 0.487 mole-e^-/cc when packed to a physical density of 1 g/cc) with a wide particle-size variation. These powders have Z_e and values that are less than water (whose Z_e = 7.43 and = 0.555 mole-e^-/cc). Tartaric acid and lithium carbonate are safe to handle and they can be packed to match the physical density of water.

Table 1 identifies the actual tartaric acid and lithium carbonate powders that were used along with their source information including lot number and how they were prepared. In an effort to evaluate varied particle size of tartaric acid, a portion of the tartaric acid was used as received from the vendor with large particle sizes (called *large-particle*), another portion was *medium-milled* using a mortar and pestle to a medium particle size, and a third portion was *fine-milled* using a ball mill to a fine particle size. Both types of milled powders were delumped using a sieve as given in Table 1 prior to use. The lithium carbonate was only used as received; it was not milled.

Table 1. Description of the powders used in this study.

Powder	Source	Lot #	Comments
DL-tartaric acid ($C_4H_6O_6$)	Sigma Aldrich	MKBG7822V	Medium-milled: Milled and delumped through US 30 mesh screen Fine-milled: Milled and delumped through US 18 mesh screen
		MKBJ6801V	Large-particle: Used as received
Lithium carbonate (Li_2CO_3)	Sigma Aldrich	BCBG9304V	Used as received

Scanning Electron Microscope (SEM) images of the tartaric acid both as received and after fine-milling using a ball mill are shown in Figure 1. Figure 2 shows SEM images of lithium carbonate as received. These images illustrate the particle morphology and qualitative particle size. Note that each of the images was taken with a different magnification.

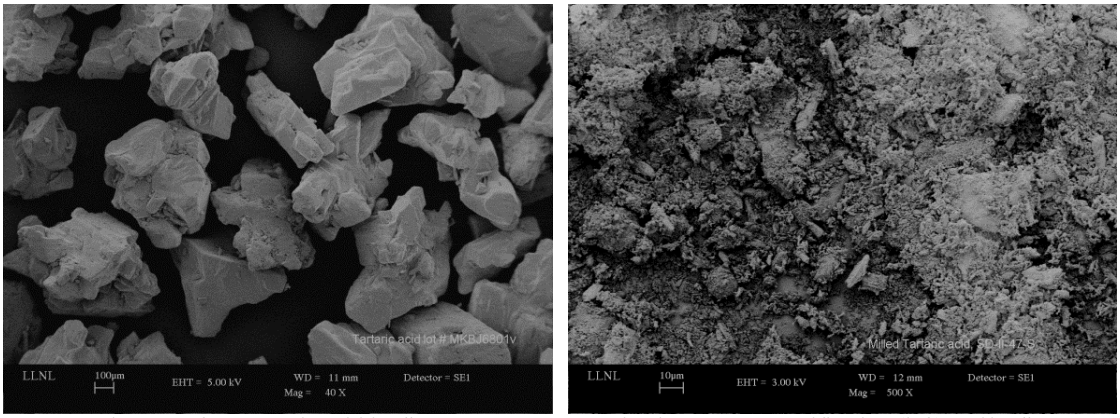

Figure 1. SEM images of DL-tartaric acid lot # MKBJ6801V as received at a 40X magnification (left) and lot # MKBG7822V fine-milled at a 500X magnification (right).

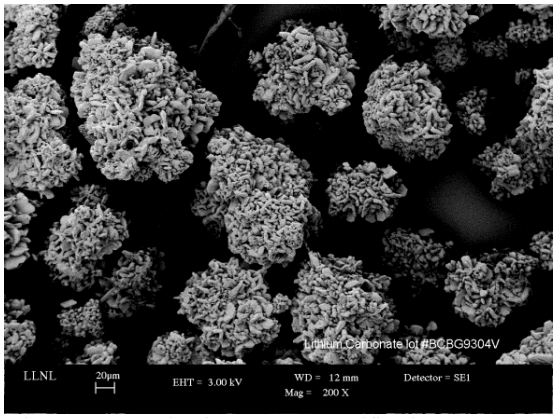

Figure 2. SEM image of lithium carbonate (as received) at 200X magnification.

The distribution of particle size in these powders can be measured using a Micromeritic low volume Saturn Digisizer 5200. Figure 3 shows the particle size distributions measured with this method for the two lots of tartaric acid as received from the vendor. They exhibit similar bimodal particle size distributions.

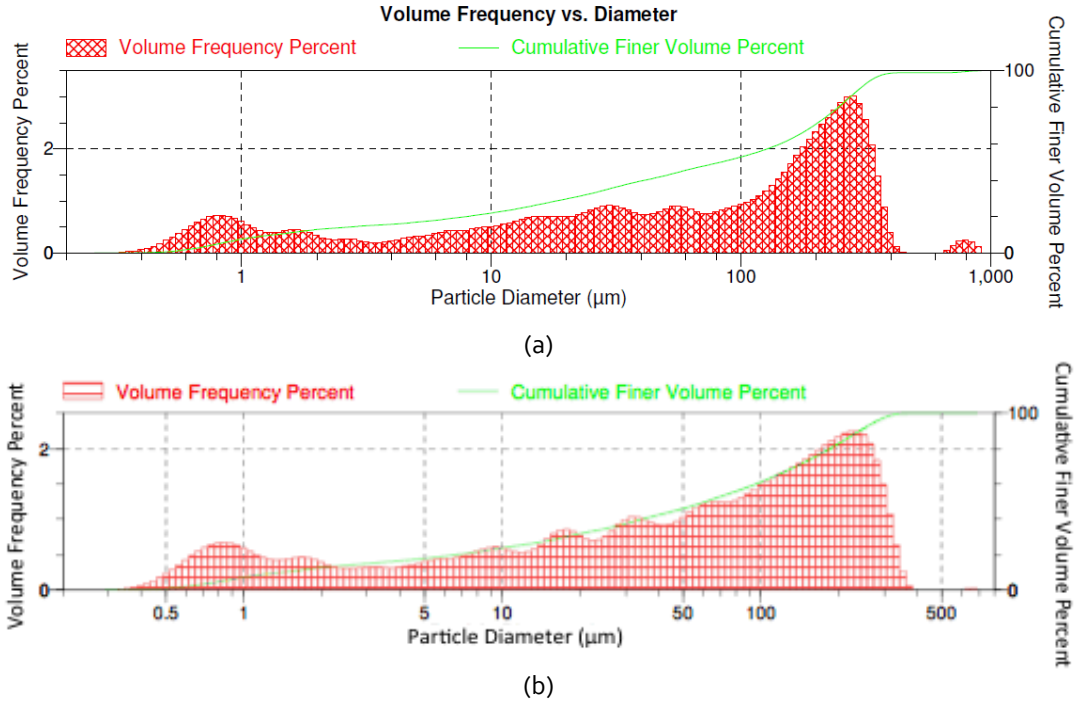

Figure 3. Particle size distribution for as-received tartaric acid from (a) lot # MKBJ6801V with mean particle size of 44 µm and (b) lot # MKBG7822V with mean particle size of 35 µm.

Due to the material availability, one lot of tartaric acid (MKBJ6801V) was used as received from the vendor while the other (MKBG7822V) was milled to medium-milled and fine-milled powders as described in Table 1. After milling, the particles size distributions changed as expected as shown in Figure 4.

The as-received lithium carbonate particle size was also characterized by the same technique. The results are shown in Figure 5. It has a different bimodal particle size distribution with modes at ~9 and ~100 µm and a mean particle size of 45 µm.

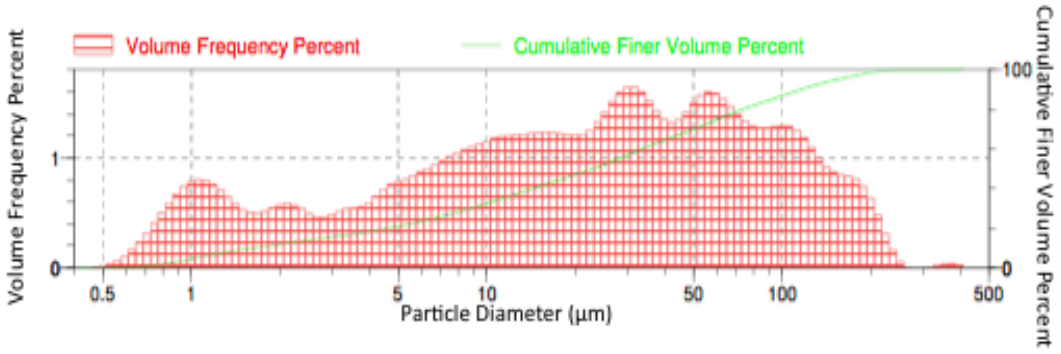

(a)

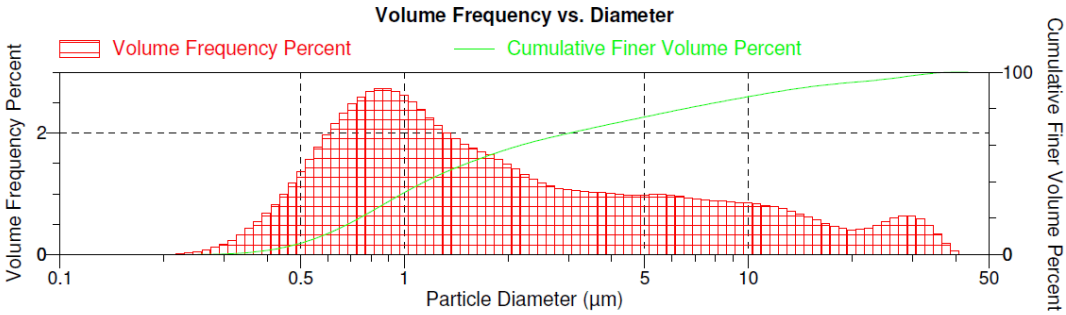

(b)

Figure 4. Particle size distribution for tartaric acid (lot # MKBG7822V) that was (a) medium-milled to a mean particle size of 18 µm and (b) fine-milled to a mean particle size of 2 µm.

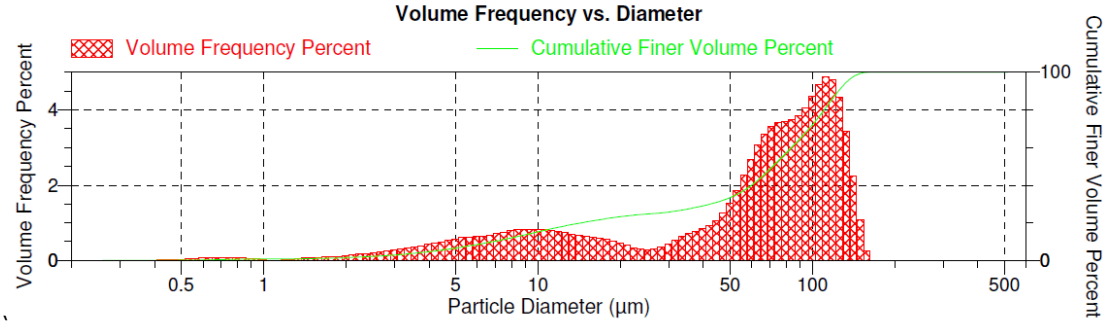

Figure 5. Particle size distribution lithium carbonate as received. The bimodal particle size distribution has modes at ~9 and ~100 µm and a mean particle size of 45 µm.

5. SPECIMEN PREPARATION

The as-received lithium carbonate (LC) and the three particle sizes of tartaric acid (TA) were separately packed into 250-ml Nalgene bottles using two types of packing methods described below. An example tartaric acid specimen ready for CT scanning is shown in Figure 6. For reference to the CT images, "vertical" and "horizontal" image slices refer to the specimen bottle as though it is standing upright as in Figure 6 regardless of the bottle's orientation during scanning; horizontal slices have a circular cross section.

Figure 6. Example specimen consisting of a 250-ml Nalgene specimen bottle packed with tartaric acid.

1. Tap Packing Method

Tartaric acid and lithium carbonate were prepared with a *tap packing* method. Using this method, the powder was loaded into the specimen bottle while tapping the container lightly on the bench top. The bottle was filled completely and then placed on a Quantachrome autotap instrument where it was tapped (dropped) automatically 1000 times at 260 drops/minute with a 1/8-inch drop height.

2. Heavy-Tamp Packing Method

Tartaric acid and lithium carbonate were prepared with a *heavy-tamp packing* method. Using this method, the powder was loaded into the specimen bottle in approximately 30-35 g layers. After each layer was added to the container, a 1.2-inch diameter Teflon tamper was used to lightly tamp down the fluffy powder before doing the heavy tamping. For heavy-tamp packing, the bottle of powder was placed on a scale and the preparer pushed down on the 1.2 inch tamper (with an off center rod to get under the shoulder of the bottle) with about 30 pounds of force and a three-second hold. This pressure with the tamper was repeated 16 times while rotating the tamper relative to the bottle, before adding the next layer of powder. Multiple layers of powder were added until the shoulder of the bottle was nearly reached. Tartaric acid was packed in 7 layers. Lithium carbonate was packed with 6 layers. The difference is due to slightly different packing densities and the amount that would fit into the 250-ml container.

6. PHYSICAL DENSITY DETERMINATION

After each specimen was prepared, its bulk physical density was determined by measuring the weight and volume of powder in the 250-ml Nalgene bottle. The powder weight was calculated by weighing the specimen bottle on a balance then subtracting the weight of an empty bottle. The volume was determined by filling a different but equivalent 250-ml bottle with water to the same level as the powder in the specimen bottle, weighing the water (subtracting the empty bottle weight) and then converting that number to a volume. For each type of specimen we prepared and measured three separate specimens from scratch to obtain an idea of measurement uncertainties.

We noticed that the heavy-tamped medium-milled tartaric acid specimens had a higher density than both the heavy-tamped large-particle and fine-milled tartaric acid. This has to do with the particle size distributions and how powders of different sizes pack together. The medium-milled material has a very wide particle size distribution that enables interstitial packing of smaller particles between the larger particles increasing the packing density. For this reason, it is common to use a bimodal particle size distribution to achieve increased packing/pressing densities of powders.
Another interesting phenomenon we noticed was that large-particle tartaric acid specimens have a higher physical density when tap packed than the medium- and fine-milled specimens. The increased density of the large-particles in this

instance is due to the better flow characteristics of this more granular material. Finer particles tend to stick together or agglomerate and do not flow as well when tapped.

7. CT DATA ACQUISITION

As described above, there were three specimens tested for each of the 8 specimen types (two packings each of three particle sizes of tartaric acid and two packings of lithium carbonate) making a total of 24 specimens. All specimens were scanned on the MicroCT scanner. This scanner is located in the LLNL High Explosives Application Facility (HEAF) near the formulation and preparation lab. The CT scanning protocol was the same for each specimen.

.

The MicroCT scanner system is designed to measure and compare the physical properties of samples in the context of computed-tomographic imaging. The scanner includes a high-resolution high-voltage DC x-ray source, an area detector, a positioning system that provides "rotate-only" imaging, a specimen support stage and a double-slit collimator (see Figure 7).

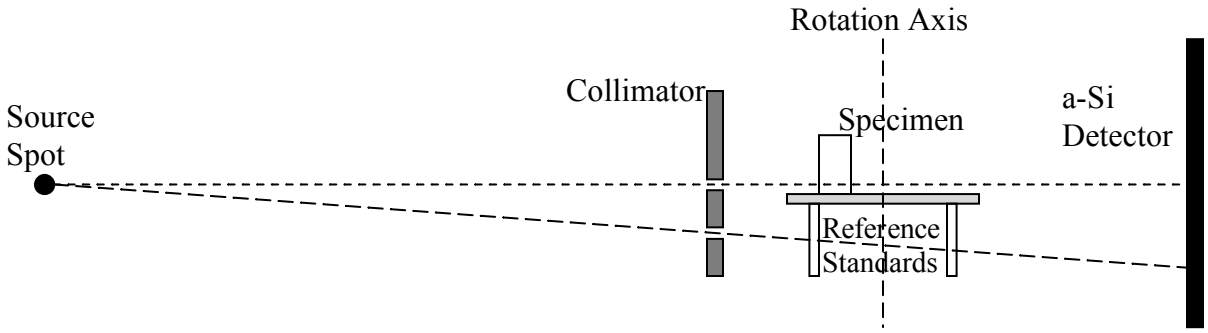

Figure 7. Micro-CT System Geometry : The specimen is viewed through the upper specimen slit in the collimator and the reference standards are viewed through the lower reference slit. The upper part of the collimator can be removed to view the full specimen in a "single-slit" configuration.

There are two planes imaged by the MicroCT through the two collimator slits. The upper plane, through a "specimen slit," illuminates a single specimen which is the unknown material to be characterized. The lower plane, through a "reference slit," incorporates a number of known "reference standards" - pure materials that span the density/Z_e space that are used for calibration and for monitoring the stability and consistency of the imaging system. The two-slit collimator projects two x-ray fan beams, one through each plane, while minimizing out of plane detector blur and x-ray scatter from outside those fans. These fan-beam data are reconstructed as 2-D images.

A single-slit (open) MicroCT configuration employs the same reference slit, but the specimen-slit collimator is removed in order to image nearly the complete specimen volume. The single-slit configuration provides information about the volume variation in a specimen at the expense of ~5% out-of-slice detector-blur contamination. Therefore, the quantitative CTN measurements in this study were performed on the lower-blur dual-slit data: we only used single-slit data to correct the physical density variations in the bottle as described later in section 9.2. For this configuration, most of the upper part of the specimen bottle is blocked from the x-rays to minimize detector blur; only the bottom ~2% of the bottle is illuminated through the specimen slit.

A prepared specimen was first taken to the MicroCT system in HEAF in an upright position and carefully mounted on the carousel. Each specimen was scanned two times by the MicroCT system, and both scans occurred on the same day. The two MicroCT scans had the following configurations:

- Dual-slit with 160 kVp source filtered with Al/Cu (160AlCu);
- Single-slit (Open) with 160 kVp source filtered with Al/Cu (160AlCu1slit).

8. CT IMAGES

The CT scanner data sets were reconstructed to generate 3D voxelized images of the specimen bottles. Extracted orthogonal 2D image slices of one specimen (tartaric acid, small particle, hard packed) are shown in Figure 8. The image voxels are arbitrarily scaled to be square and to display the full specimen.

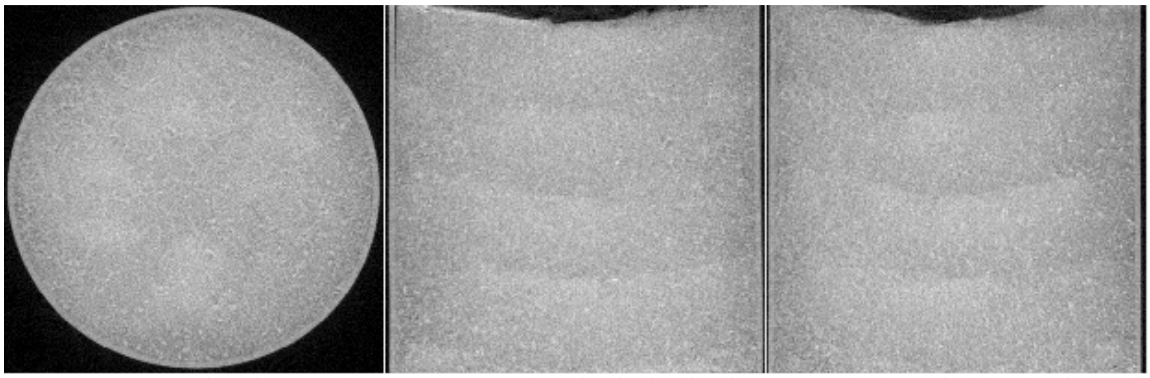

Figure 8. Reconstructed CT images of TA_SH01 scanned on the single-slit MicroCT. A horizontal midsection image is at left and two orthogonal vertical images are center and right. The specimen slit for dual-slit MicroCT covers the bottom ~2% of the vertical images.

The MicroCT raw data were reconstructed into CT images and converted to LMHU. Single-slit data resulted in 3D voxelized attenuation files of the specimen volume like the one represented by three slices in Figure 8. The specimen itself occupies about 400-500 million voxels that are about 0.15 mm on each side. About 300 horizontal image slices (like the left image in Figure 8) are generated by the single-slit MicroCT. Dual-slit MicroCT has the same voxel size, but collimates the X-rays to only illuminate and reconstruct the bottom seven slices of the associated single-slit data. Because of the mounting geometry and interference with the stage, neither configuration of MicroCT images the bottom few millimeters of the bottle.

9. DATA ANALYSIS

This section describes the steps that were performed in the analysis of the data.

1. Mean CTN Estimation

After reconstruction MicroCT volumes were processed to estimate a scalar-valued mean CTN for the imaged powder specimen. For completeness, estimates of higher-order statistics such as standard deviation and entropy were calculated and stored as well. The first step was to convert voxelized attenuation values to LMHUs using a water reference standard. For the MicroCT, voxels are converted to LMHU using the water reference standard that is simultaneously scanned with the specimen, but in the lower slit.

For the MicroCT scanner, the mean CTN estimation was performed on the seven dual-slit specimen slices. This process involves identifying the powder within the specimen slit, reducing each slice area to ~85% to eliminate the container and partial volume effects (by 15 morphological erosions using a 3x3 structuring element) and calculating the statistics of the remaining voxels. The resulting specimen voxels in the slices are averaged to obtain the mean CTN of the powder.

2. Correction for Vertical Density Variations

The mean CTN estimate for dual-slit MicroCT is only accurate for the small specimen-slit volume, which is only ~2% of the entire specimen volume near the bottom of the bottle as described in the Section 7. Thus, when comparing this mean CTN to physical density it is important to use the physical density of that 2% specimen-slit region. However, due to the way powders are packed into the bottle, the powder at the bottom of the bottle can have a very different physical density compared to the overall volume density as measured in Section 6. How do we estimate the physical density of the specimen-slit region alone given this vertical variation in physical density?

This correction can be done using the single-slit MicroCT images like the one shown in Figure 8 of the full specimen volume. From these images, we can calculate the mean CTN for each horizontal slice from top to bottom to generate a plot such as that shown in Figure 9 for a medium particle size, tapped tartaric acid specimen, which has more vertical density variation than most specimens so the effect is easily seen. With respect to the curve in Figure 9, the x-axis values from left to right indicate the image slice number from the top to bottom of the specimen bottle. The equivalent specimen-slit location for the dual-slit MicroCT scan is highlighted in yellow near the bottom of the bottle. The blue curve reveals a slope of increasing mean CTN toward the bottom of the bottle. All of the packed powder specimens exhibited this behavior to some degree.

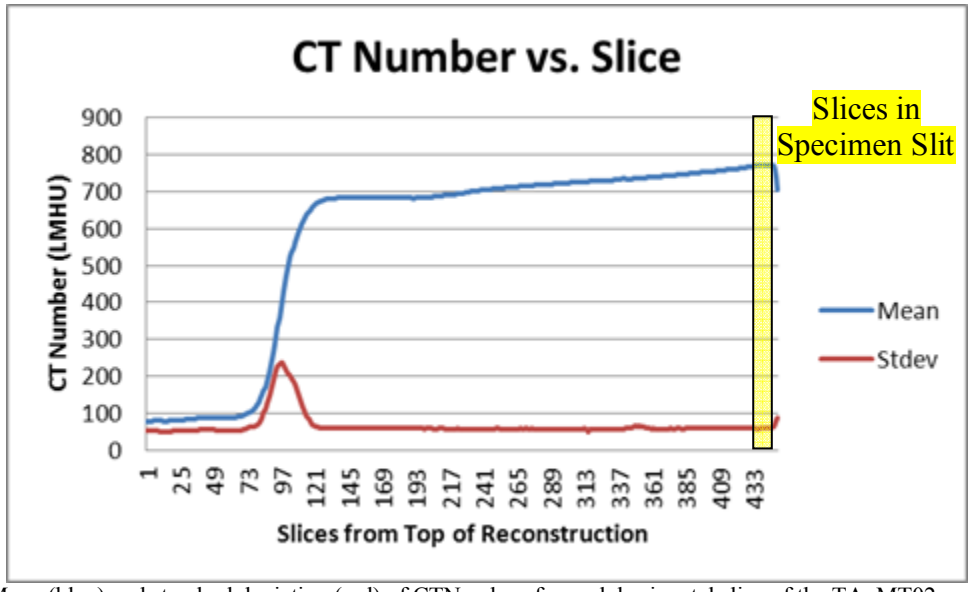

Figure 9. Mean (blue) and standard deviation (red) of CTN values for each horizontal slice of the TA_MT02 specimen bottle scanned on single-slit MicroCT. The slice numbers on the x-axis are from the specimen bottle top (about slice 76) to bottom (about slice 450). The equivalent specimen-slit location for dual-slit MicroCT is at the bottom of the bottle highlighted at right in yellow.

Since each specimen is a single powder—i.e., with the same Z_e and the same powder characteristics—and the bottle diameter is constant over most of the powder specimen[1], this slope in mean CTN is attributable to increased physical density from top to bottom. In this case of TA_MT02, the top to bottom density difference is approximately 8.5%. Therefore, from the single-slit MicroCT results in Figure 9 we have a relative measure of the vertical density variations. The following correction to the volume physical density measurement provides an estimate of the physical density in the specimen slit alone for comparison to dual-slit MicroCT:

$$\text{Physical density}_{\text{in slit}} = \left(\frac{\text{mean CTN in specimen slit}}{\text{mean CTN in full volume}}\right)(\text{Physical density}_{\text{in volume}}) . \quad (4)$$

This formula was used to correct the physical density and these corrected physical densities were used in the analysis of dual-slit MicroCT data and also to calculate electron densities in the specimen slit.

[1] We considered the top of the powder sample itself to be where the standard deviation returns to baseline (around slice 126 for the specimen in Figure 9).

10. RESULTS

1. Effects of Powder Properties (Density)

- Why do powders whose physical properties (effective atomic number, Z_e, and density) are near water produce CTNs that do not match those of water?

We plot the tartaric acid and lithium carbonate CTN values from the MicroCT against physical density in Figure 10. We use the corrected physical density describe in the Section 2.

The clusters of three specimens of the same type are well separated so we can see the variability in formulation and measurement as well as trends between specimen types. A single water data point is also plotted on each figure for reference. The water point is the average of several water specimens separately scanned in the specimen-slit position on the MicroCT (rather than using the water reference standards used for conversion to CTN).

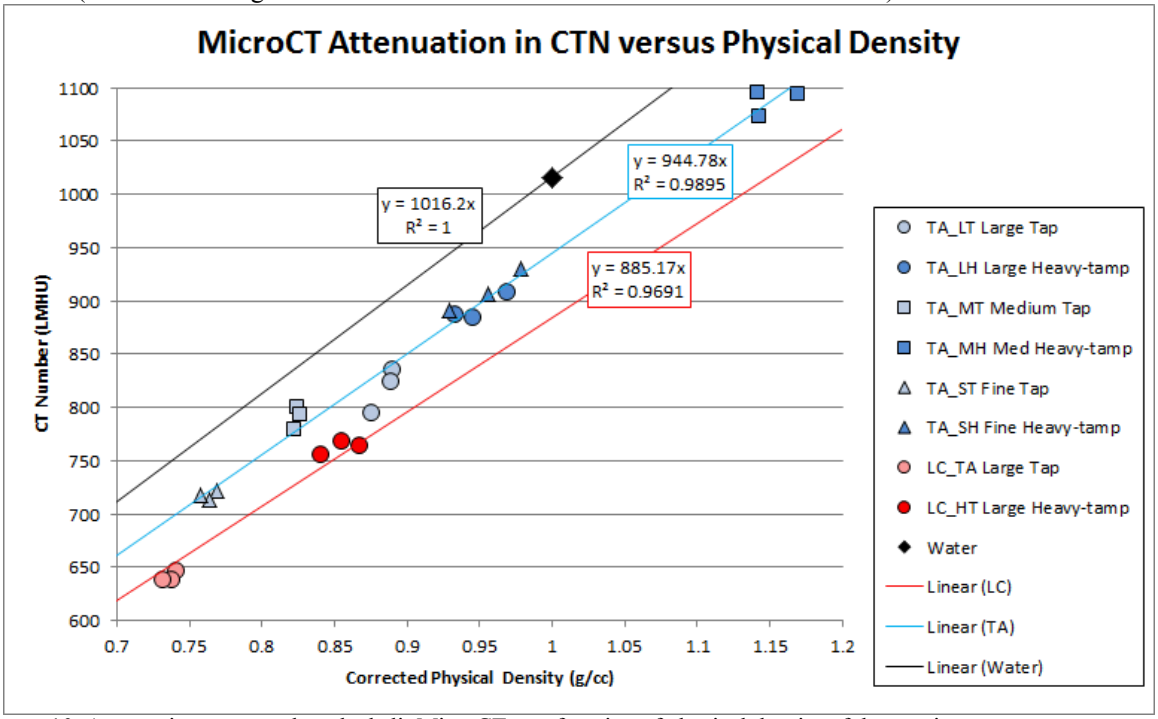

Figure 10. Attenuation measured on dual-slit MicroCT as a function of physical density of the specimens.

We plot linear trend-lines for the two powders and for water separately because the data clusters indicated this separation. All three lines are plotted with a zero y-intercept because any materials with near-zero density (e.g., air) are set to zero CTN as implied in Equations 1-3. The slopes of these lines are shown in the colored boxes and can be thought of as the powder characteristics factor M introduced in Equation 2. The coefficients of determination (R^2) are close to one in each case, indicating a good linear regression fit (R^2=1 means all points lie exactly on the same line).
Figure 10 confirms that the trend lines for the two powders in this study are lower than the expected water line predicted by Equation 1. They also show that if Equation 2 is the correct model then the morphology factor, M, is different for these two powder materials.

The alternative hypothesis is that the CTN is a function of electron density as in Equation 3. To test this hypothesis we produced the same plot, but as a function electron density. Electron densities of the powder specimens were computed by multiplying the electron density of the powder at 1g/cc (calculated by ZeCalc [Bond1]) against the corrected physical density. We are effectively scaling the calculated electron density by the measured physical density as in Equation 5.

(5)

The resultant plot is shown in Figure 11. In this case, the specimen clusters for the two powders and water are nearly co-linear, so we display only one trend line, which demonstrates a good regression fit. This shows that the majority of the CTN reduction of powders is due to the disparity between the electron density of water and the electron density of the powders when packed to 1 g/cc.

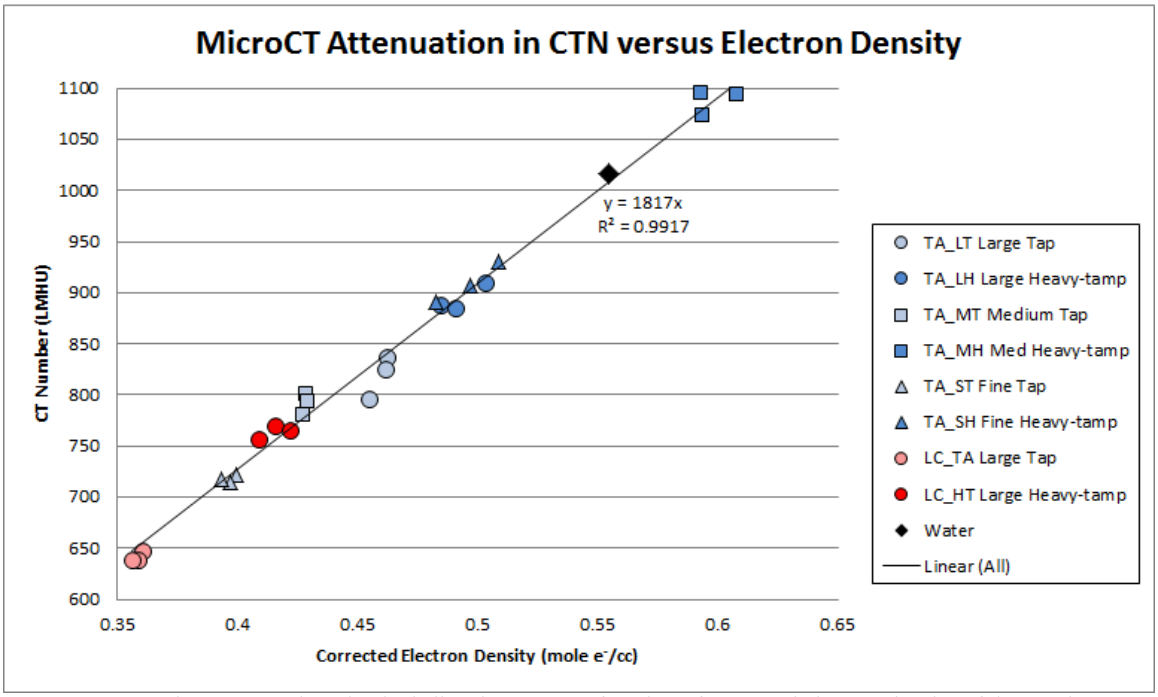

Figure 11. Attenuation measured on the dual-slit MicroCT as a function of corrected electron density of the specimens.

Notice that all specimens fall on the same line as water when plotted against electron density as implied by Equation 3. Figures 10 and 11 illustrate that attenuation or CTN values are related to electron density rather than bulk physical density for these powders. While the linear fit is remarkably good for these specimens whose Z_e values are within ±0.2 of water, more expanded tests would be needed to investigate the CTN dependence on at greater ranges of Z_e values and physical densities.

2. Effects of Morphology and Particle Size

- How do morphology and particle size of powders affect CTN values?

While the 10.1 addressed how density affects CTN (there is a linear relationship with electron density), this section explores the effects of morphology and particle size on CTN for a given density. We can do this with the same data by focusing on one cluster of specimens.

Let us compare the CTNs of specimens with two different particle sizes packed to the similar corrected physical densities. Examples are the heavy-tamped large-particle and fine-milled tartaric acid specimens, which are tightly clustered in Figures 9 and 10. From these points, we can calculate the mean-of-means and the standard-deviation-of-means to produce two-sided statistical tolerance limits for these specimens as shown in Figure 12. The square regions around the specimen clusters are the two-sided statistical tolerance limits[3] for the two powder particle size distributions packed to nearly the same densities. They are created from the sample standard deviation multiplied by a factor to achieve 90% confidence that 90% of the time a new specimen will fall within the box.

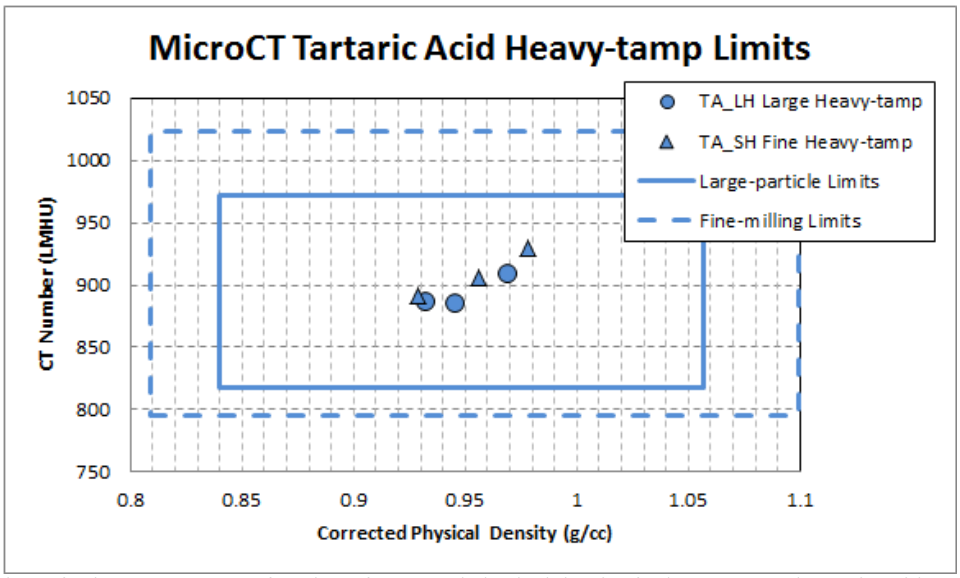

Figure 12. Plots of MicroCT CTN as a function of corrected physical density for heavy-tamped tartaric acid specimens with two different particle sizes (large-particle and fine-milled).

While it is difficult to make quantitative statements with so few measurements, the key point of this plot is that all six specimen points lie within both sets of tolerance limits. Therefore, given these statistical tolerance limits, there is no major difference in CTN between large-particle and fine-milled specimens as long as they are packed to the same physical density.

We conclude that the effects of morphology and particle size on CTN are negligible. Regardless of particle size and structure, as long as the material and its physical density are the same then MicroCT estimates of mean CTN will be the same to within statistical tolerance limits.

11. SUMMARY

Two powder materials were milled to several particle sizes and packed into 24 specimens of several physical densities that were independently measured. The specimens were then scanned by the MicroCT system, and the data were analyzed to study the effects of powder characteristics on X-ray attenuation or CTN. Our experiments have shown that

- For powders whose Z_e difference is within ±0.2 of water, CTN has a better functional relationship to *electron* density than to *physical* density.
- Variations in powder morphology and particle sizes studied here, when packed to the same physical density, had little effect on the mean CTN value.

12. FUTURE WORK

Future work may include an expanded study of materials with greater Z_e ranges, greater physical density variations (such as foams), and powders with multiple components of disparate Z_e.

13. ACKNOWLEDGEMENTS

This work was supported by DHS S&T. The authors would like to acknowledge the efforts of Bill Brown, Denise Grimsley, Kenn Morales, Jennifer Montgomery, Isaac Seetho, Pat Roberson, Travis White and Audrey Williams for their help in preparing the specimens, generating the X-ray data and analyzing the results described in this report.

14. DISCLAIMER AND AUSPICES

This work performed under the auspices of the U.S. Department of Energy by Lawrence Livermore National Laboratory under Contract DE-AC52-07NA27344.

15. REFERENCES

[1] K. C. Bond, J. N. Treuer, S. J. Azevedo, J. S. Kallman, H. E. Martz and J. A. Smith, "ZeCalc Algorithm Details (Version 1.1)," LLNL-TR-609327, (2013).
[2] J. A. Smith, "Ze: An Effective Atomic Number for Polychromatic X-ray Transmission," LLNL-JRNL-640273, July 2013. Submitted to Nuclear Instruments and Methods in Physics Research, Section B.
[3] M. G. Natrella, [Experimental Statistics], National Bureau of Standards Handbook 91, 2-13 – 2-15 (1963).